Density Functional Description of the Ferromagnetic Exchange Interactions between Semiquinonato Radicals Mediated by Diamagnetic Metal Ions

Alessandro Bencini,* Ilaria Ciofini, and Elisa Giannasi

Dipartimento di Chimica, Università di Firenze, Firenze, Italy

Claude A. Daul and Karel Doclo

Institut de Chimie Inorganique et Analytique, Université de Fribourg, Fribourg, Switzerland

Received July 24, 1997

The electronic structures of $Ti(CatNSQ)_2$ and $Sn(CatNSQ)_2$, where $CatNSQ^{2-}$ is the tridentate radical ligand (3,5-di-*tert*-butyl-1,2-semiquinonato 1(2-hydroxy-3,5-di-*tert*-butyl-phenyl)immine), were investigated with density functional (DF) calculations, using the local approximation for the exchange-correlation functional. The crystal structure of $Sn(CatNSQ)_2$ was solved. The complex crystallizes in the orthorhombic space group, $C222_1$, with $Z = 8$ in a unit cell of the following dimensions: $a = 19.580(5)$ Å, $b = 24.310(5)$ Å, $c = 23.690(5)$ Å. The crystals are not isomorphous with similar $M(CatNSQ)_2$ (M = Ti, V) complexes previously reported. DF calculations showed that the triplet ($S = 1$) spin state is stabilized with respect to the first excited singlet ($S = 0$) state and the computed exchange coupling constant J is in semiquantitative agreement with the values obtained from magnetic susceptibility measurements. Using a symmetry-based multiplet structure decomposition in terms of states defined by a single determinant (single determinant method, SD) the energies of the excited singlet states were also computed in agreement with the experimental data. The calculations have shown that the main exchange mechanism between the organic radicals, responsible for the ferromagnetism of these complexes, is a superexchange pathway mediated by the 3d orbitals of Ti and the 4p empty orbitals of Sn. Magnetostructural correlations between the exchange coupling constant and the M−O and M−N bond distances have been established.

Introduction

Exchange interactions between organic radicals are currently under investigation by material chemists who continuously synthesize new compounds with the aim of stabilizing ferromagnetic interactions and extending the interactions to long-range order.[1−4] In general, organic molecules are closed-shell systems and possess no net magnetic moment. In the case of pure organic radicals, often antiferromagnetic interactions are observed due to the overlap between the magnetic orbitals localized onto adjacent molecules in the solid state. In a few cases ferromagnetic interactions between stable organic radicals have been measured, for example, in galvinoxyl,[5] nitronyl nitroxides[6] or polycarbenes[7−10] and polyarylmethyl.[11] Binding metal ions to organic radicals has been a synthetic route followed to investigate the possibility of stabilizing ferromagnetic states. In particular nitronyl nitroxide−transition metal or −rare earth complexes have been prepared and studied.[12,13] Another kind of organic radicals which can bind to metal ions are the polyoxolene radicals, and a number of complexes have been synthesized and studied.[14] Most often the high-spin state, resulting from parallel alignment of the unpaired electrons localized on the metal center and those on the radical ligands, is the ground state of the system. The high-spin state can be stabilized by hundreds of wavenumbers, giving rise to ferromagnetic interactions larger than those observed in nitronyl nitroxide systems. For these reasons metal−polyoxolene systems have been regarded as potential candidates for obtaining bulk ferromagnets.

The description of the electronic structure of metal−polyoxolenes is a rather complicated matter, since charge transfer states, both metal-to-ligand and ligand-to-metal, are near to the ground state and are responsible for variation of the formal oxidation state of the metal with temperature and related phenomena. The tridentate ligand (3,5-di-*tert*-butyl-1,2-semiquinonato 1(2-hydroxy-3,5-di-*tert*-butyl-phenyl)immine), $CatNSQ^{2-}$, derived by the reaction between 3,5-di-*tert*-butyl-1,2-semiquinone and 3,5-di-*tert*-butyl catecholato with ammonia,

(1) Miller, J. S.; Epstein, A. J.; Reiff W. R. *Acc. Chem. Res.* **1988**, *21*, 114.
(2) Kahn, O. *Angew. Chem., Int. Ed. Engl.* **1985**, *24*, 834.
(3) Caneschi, A.; Gatteschi, D.; Sessoli, R.; Rey P. *Acc. Chem. Res.* **1989**, *22*, 392.
(4) Gatteschi, D., Kahn, O., Miller, J. S., Palacio, F., Eds. *Magnetic Molecular Materials*; Kluwer: Dordrecht, The Netherlands, 1991.
(5) Awaga, K.; Sugano, T.; Kinoshita, M. *Solid State Commun.* **1986**, *57*, 453.
(6) Awaga, K.; Maruyama, Y. *J. Chem. Phys.* **1989**, *91*, 2743.
(7) Sugawara, T.; Bandow, S.; Kimura, K.; Iwamura, H.; Itoh, K. *J. Am. Chem. Soc.* **1986**, *108*, 368.
(8) Teki, Y.; Takui, T.; Itoh, K.; Iwamura, H.; Kobayashi, K. *J. Am. Chem. Soc.* **1986**, *108*, 2147.
(9) Fujta, I.; Teki, Y.; Takui, T.; Kinoshita, T.; Itoh, K.; Miko, F.; Sawaki, Y.; Iwamura, H.; Izuoka, H.; Sugawara, T. *J. Am. Chem. Soc.* **1990**, *112*, 4074.
(10) Veciana, J.; Rovira, C.; Armet, O.; Domingo, V. M.; Crespo, M. I.; Palacio, F. *J. Am. Chem. Soc.* **1991**, *113*, 2552.
(11) Rajca, A.; Utamapanya, S. J. *J. Am. Chem. Soc.* **1993**, *115*, 2396.
(12) Benelli, C.; Caneschi, A.; Gatteschi, D.; Pardi, L. In *Magnetic Molecular Materials*; Gatteschi, D., Kahn, O., Miller, J. S., Palacio, F., Eds.; Kluwer: Dordrecht, The Netherlands, 1991; p 233.
(13) Caneschi, A.; Gatteschi, D.; Rey, P. *Prog. Inorg. Chem.* **1991**, *39*, 331.
(14) Dei, A.; Gatteschi, D. *Inorg. Chim. Acta* **1992**, 813.

S0020-1669(97)00906-3 CCC: $15.00
Published on Web 07/03/1998

Chart 1

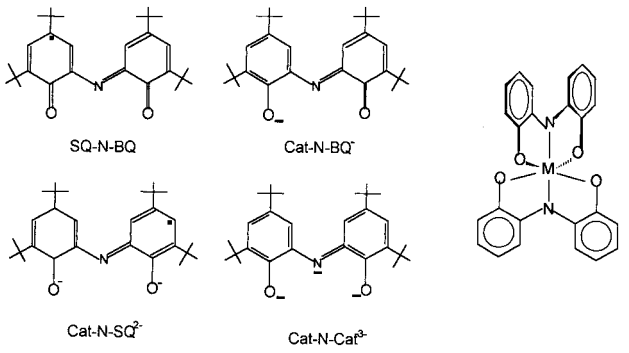

recently has been studied extensively, and a number of complexes with metal ions have been reported.[15−17] Different forms of the complexes such as $M^{IV}(CatNSQ)_2$, $M^{II}(CatNBQ)_2$, or $M^{III}(CatNBQ)(CatNSQ)$, where $CatNBQ^-$ is the diamagnetic quinone corresponding to $CatNSQ^{2-}$, have been observed and characterized spectroscopically.[16,17] A schematic view of the ligand and of the complexes is shown in Chart 1.

Quite recently a series of complexes of formula $M^{IV}(CatNSQ)_2$ (M = Ti, V, Ge, Sn) have been synthesized, and their spectromagnetic properties have been measured.[18] In the case of the Ti and Sn derivatives, in which the metals bear no unpaired electrons in the formal oxidation state IV, a ferromagnetic coupling between the unpaired electrons was observed which stabilizes the triplet state of about 50 cm^{-1} with respect to the singlet.

The interaction between two magnetic centers is generally ascribed to two main factors: the exchange energy between electrons of equal spin, which favors the parallel alignment of the spins between adjacent centers (the so-called potential exchange in the Anderson theory), and the overlap between the magnetic orbitals, which favors the antiparallel alignment of the spins (the so-called kinetic exchange in the Anderson theory).[19,20] Together with spin polarization effects, these are commonly called magnetic interactions, although electrostatic in nature, and are generally used by magnetochemists to rationalize the magnetic properties of paramagnetic molecules.[20] In the active electron approximations, only the spatial distribution of the magnetic electrons (those which occupy the molecular orbitals at higher energy) is considered and has led to the so-called exchange pathways: when the unpaired electrons are in orbitals (the magnetic orbitals) which can efficiently overlap, an antiferromagnetic interaction is expected (the $S = 0$ state is more stable than $S = 1$); when they are in magnetic orbitals which are orthogonal to each other, but have nonzero differential overlap in a sizable region of space (e.g., delocalization onto the bridging ligands), a ferromagnetic interaction occurs (the $S = 1$ state is more stable than $S = 0$).[20,21] These exchange pathways or mechanisms can be quantitatively described in a Hartree−Fock (HF) formalism, where they appear as post-HF corrections to the total energy in the configuration interaction (CI) scheme.[20] In DF calculations,[22] only the exchange coupling constant, J, defined as the energy difference between the triplet and the singlet state, can be computed, and the exchange pathways can be understood only pictorially by looking at the composition of the magnetic orbitals.[20] The advantage, however, of using the DF formalism[22] instead of ab initio ones is that the properties of large molecular systems (increasingly more similar to the real chemical systems) can be computed with reasonable computational expense and with an overall satisfactory agreement with the experimental observables.[23] It is experimentally well-known that the measured exchange coupling constants are largely affected by small deviations in bond angles and distances often bound to solid state effects and to the nature of the counterions.[24] These structural deformations cannot be handled by optimizing the geometries of the complexes in the gas phase. Therefore, calculations on magnetic systems either look for magnetostructural correlations or make use of experimental geometries (or averaged experimental geometries) rather than the geometries obtained by geometrical minimization to calculate the absolute J values to compare with the experiment. Also some idealization of the symmetry of the molecule is often done in order to limit the number of geometrical parameters to be varied. This procedure has been applied both in DF[25,26] and in ab initio calculations[27,28] on magnetic systems containing transition metal ions and transition metal ion−nitroxide radicals.

To gain a better insight into the electronic structure of the $M^{IV}(CatNSQ)_2$ complexes and into the mechanisms responsible for the exchange interaction, we have performed density functional (DF)[22] calculations of the electronic structure of the $Ti(CatNSQ)_2$ and $Sn(CatNSQ)_2$ complexes. Since the geometrical parameters of the tin derivative are not known, we have measured the X-ray diffraction pattern of $Sn(CatNSQ)_2$ and solved its crystal and molecular structure. In the present paper we report the crystal and molecular structure of $Sn(CatNSQ)_2$ and the DF characterization of the electronic structure of the titanium and tin derivatives, paying particular attention to the exchange pathways which stabilize the triplet state and to the dependence of the singlet−triplet energy gap on geometrical and bonding parameters.

Experimental Section

Crystallographic Structure Determination. Single-crystal diffraction data for $Sn(C_{28}H_{40}NO_2)_2$ were collected at room temperature on an Enraf-Nonius CAD4 four-circle diffractometer by using Mo Kα radiation ($\lambda = 0.710\ 69$ Å). Cell parameters were obtained from least-squares fits to the settings of 25 reflections centered in the range $3° \leq \theta \leq 25°$. Details on crystal data, intensity collection, and refinement are reported in Table 1. The intensities have been corrected for Lorentz−polarization effects.

The structure was solved by direct methods using the SIR92 package.[29] A good set of atomic parameters for the tin atom was

(15) Girgis, A. Y.; Balch, A. L. *Inorg. Chem.* **1975**, *14*, 2724.
(16) Larsen, S. K.; Pierpont, C. G. *J. Am. Chem. Soc.* **1988**, *110*, 1827.
(17) Simpson, C. L.; Boone, S. R.; Pierpont, C. G. *Inorg. Chem.* **1989**, *28*, 4379.
(18) Bruni, S.; Caneschi, A.; Cariati, F.; Delfs, C.; Dei, A.; Gatteschi, D. *J. Am. Chem. Soc.* **1994**, *116*, 1388.
(19) Anderson, P. W. *Solid State Phys.* **1963**, *14*, 99.
(20) Kahn, O. *Molecular Magnetism*; VCH Publishers: New York, 1993.
(21) Charlot, M. F.; Journaux, Y.; Kahn, O.; Bencini, A.; Gatteschi, D. *Inorg. Chem.* **1986**, *25*, 1060.
(22) Parr, R. G.; Young, W. *Density Functional Theory of Atoms and Molecules*; Oxford University Press: New York, 1989.
(23) *Recent Advances in Density Functional Methods*; Chong, D. P., Ed.; World Scientific: Singapore, 1995; Part I.
(24) *Magneto Structural Correlations in Exchange Coupled Systems*; Gatteschi, D., Kahn, O., Willet, R., Eds.; NATO Adv. Studies, Series C, Vol. 140; Reidel: Dordrecht: The Netherlands, 1985.
(25) Barone, V.; Bencini, A.; Daul, C. A.; Doclo, K.; Fantucci, P.; Totti, F. *Inorg. Chem.* **1997**, *36*, 5022.
(26) Noodleman, L.; Peng, C. Y.; Case, D. A.; Mouesca, J. M. *Coord. Chem. Rev.* **1995**, *144*, 199.
(27) (a) Miralles, J.; Daudey, J. P.; Caballol, R. *Chem. Phys. Lett.* **1992,** *198*, 555. (b) Miralles, J.; Castell, O.; Caballol, R.; Malrieu, J. P. *Chem. Phys.* **1993**, *172*, 33. (c) Castell, O.; Miralles, J.; Caballol, R. *Chem. Phys.* **1994**, *179*, 377.
(28) (a) Wang, C.; Fink, K.; Staemmler, V. *Chem. Phys.* **1995**, *201*, 87. (b) Fink, K.; Fink, R.; Staemmler, V. *Inorg. Chem.* **1994**, *33*, 6219.

Table 1. Crystal Data and Experimental Parameters for $Sn(CatNSQ)_2$

formula	$C_{56}H_{44}N_2O_5Sn$
fw	943.62
radiation	Mo Kα (0.71 069 Å)
temp, °C	20
cryst syst	orthorhombic
space group	$C222_1$
a, Å	19.580(5)
b, Å	24.310(5)
c, Å	23.690(5)
α, deg	90.000(5)
β, deg	90.000(5)
γ, deg	90.000(5)
V, Å^3	11276(4)
Z	8
μ, cm^{-1}	4.95
N_{meas}	6743
$N_{obs}[4\sigma(I)]$	4271
R^a	0.059
$R_w{}^a$	0.17

[a] The conventional *R* factors are $R = \sum||F_o| - |F_c||/\sum|F_o|$ and $R_w = [w(F_o - F_c)^2/wF_o^2]^{1/2}$ with *w* defined in the text.

obtained. The positions of the other non-hydrogen atoms were obtained by successive Fourier and difference Fourier syntheses using the SHELXL93[30] package. The structure was refined with the use of a full-matrix least-squares method based on minimization of the function $\sum w(|F_o| - |F_c|)^2$ with weights $w = 1/[\sigma^2(F_o^2) + (0.103P)^2 + 10.05P]$ where $P = (\max(F_o^2, 0) + 2F_c^2)/3$. Anisotropic thermal parameters were applied to all the non-hydrogen atoms. Hydrogens were introduced in calculated positions (C−H = 1.08 Å), account being taken for the proper carbon hybridization, as fixed contributions to F_c. The isotropic thermal factor for every hydrogen atom was fixed to $^3/_2$ of the corresponding carbon atom's U_{eq}. Three *tert*-butyl groups were found to exhibit a 2-fold rotational disorder, as already observed for the analogous complexes of Co, Mn, and Ti. These groups were refined with a fixed occupancy factor of 50% for the disordered atoms. All of these groups are affected by thermal motion disorder. Residual electron density was assigned to some disordered solvent molecules, probably impurities of water, and one oxygen atom was introduced disordered on two positions. The final conventional *R* factors were *R* = 0.059 and $R_w = 0.17$ for 4271 reflections and 582 parameters. The highest peak in the last difference Fourier map was 0.624 e Å^{-3}.

Selected bond lengths and angles are reported in Table 2. Tables of data collection information (SI), positional and thermal parameters (SII) for all atoms, interatomic distances and angles (SIII), and anisotropic thermal parameters (SIV) are available as Supporting Information.

Computational Details. Density functional calculations were performed with the ADF (Amsterdam Density Functional) program package, in the version 2.20.[31] The basis functions used are those given in the program database. A triple-ζ basis was applied to the valence electrons of the metals (3d and 4s for Ti; 4d, 5s, and 5p for Sn); the 4p orbitals of Ti were treated with a single-ζ basis. Valence electrons on C, N, O (2s and 2p orbitals in any case) and H (1s orbital) atoms were treated with a double-ζ basis. All of the other electrons were frozen in their core states. All of the calculations were performed in the local spin density approximation (LSDA) using the Slater functional for the exchange and Vosko, Wilk, and Nusair (VWN) functional for the correlation energies.[32] The correlation between electrons of the same spin was corrected with the Stoll (S) expression.[33]

Table 2. Selected Bond Distances (Å) and Angles (deg) for $Sn(CatNSQ)_2$

Sn1−O1	2.062(6)	Sn1−O2	2.085(7)
Sn1−O3	2.059(8)	Sn1−O4	2.074(7)
Sn1−N1	2.103(7)	Sn1−N2	2.089(7)
N1−C2	1.358(12)	N1−C16	1.370(11)
N2−C30	1.356(13)	N2−C44	1.365(12)
O1−C1	1.329(12)	O2−C15	1.318(11)
O3−C29	1.338(12)	O4−C43	1.335(12)
C1−C6	1.431(14)	C1−C2	1.412(13)
C2−C3	1.413(13)	C3−C4	1.348(14)
C4−C5	1.43(2)	C5−C6	1.34(2)
C15−C20	1.413(12)	C15−C16	1.430(14)
C16−C17	1.388(12)	C17−C18	1.357(13)
C18−C19	1.409(14)	C19−C20	1.403(14)
C29−C34	1.39(2)	C29−C30	1.425(14)
C30−C31	1.409(14)	C31−C32	1.369(14)
C32−C33	1.39(2)	C33−C34	1.40(2)
C43−C48	1.41(2)	C43−C44	1.424(14)
C44−C45	1.376(14)	C45−C46	1.364(14)
C46−C47	1.39(2)	C47−C48	1.40(2)
N2−Sn1−N1	177.7(3)	O3−Sn1−O4	153.8(3)
O3−Sn1−01	95.2(3)	O4−Sn1−O1	91.0(3)
O3−Sn1−O2	91.2(3)	O4−Sn1−O2	94.3(3)
O1−Sn1−O2	154.0(3)	O3−Sn1−N2	76.9(3)
O4−Sn1−N2	76.9(3)	O1−Sn1−N2	101.1(3)
O2−Sn1−N2	104.8(3)	O3−Sn1−N1	103.2(3)
O4−Sn1−N1	102.9(3)	O1−Sn1−N1	76.5(3)
O2−Sn1−N1	77.5(3)		

All of the calculations were performed in the spin-unrestricted formalism using the single determinant (SD) method, briefly described in the next section.

Results and Discussion

Structure of $Sn(CatNSQ)_2$ and Spectromagnetic Properties. The crystals of $Sn(CatNSQ)_2$ are orthorhombic and are not isomorphous with all of the other complexes of the series, which are triclinic. The molecular structure of $Sn(CatNSQ)_2$, however, closely resembles that of all of the other complexes of the series. The two $CatNSQ^{2-}$ radicals bind the metal atom in a tridentate fashion. The ORTEP drawing of the complex is shown in Figure 1. Selected bond distances and angles are reported in Table 2. The Sn−O bond distances are slightly longer than those observed in the other complexes of the series (2.1 vs 1.9 Å) as expected because of the larger dimensions of the metal cation. The main structural difference of the Sn derivative compared to the other ones is the deviation of the aromatic rings of the $CatNSQ^{2-}$ ligand from coplanarity. The dihedral angles between the planes are 30.4(7)° and 28.7(7)° in the two symmetry nonequivalent ligands. These figures are to be compared with the average values of 9.7° and 10° observed in the titanium and vanadium complexes, respectively.[18] The two tridentate ligands lie in almost orthogonal planes as already observed in all of the other cases. The deviation of the benzene rings from coplanarity seems to be attributable to steric interaction between the *tert*-butyl groups present on the rings as substituents. Both Ti and Sn do not possess any crystallographic symmetry, but the bond angles and distances in the chromophore do not deviate much from an idealized C_{2v} symmetry. The highest symmetry of the molecule would be D_{2d} if the O−M−O angle were 180°.

UV−vis and EPR spectra and the temperature dependence of the magnetic susceptibility of $Ti(CatNSQ)_2$ and $Sn(CatNSQ)_2$

(29) Altomare, A.; Cascarano, G.; Giacovazzo, C.; Cuagliardi, A. *J. Appl. Crystallogr.* **1994**, *27*, 1045.
(30) Sheldrick, G. M. *SHELXL-93*; Universität Göttingen: Göttingen, Germany, 1993.
(31) (a) ADF Version 2.2.0, Theoretical Chemistry, Vrije University, Amsterdam, 1996. (b) Baerdens, E. J.; Ellis, D. E.; Ros, P. *Chem. Phys.* **1973**, *2*, 41. (c) te Velde, B.; Baerdens, E. J. *J. Comput. Phys.* **1992**, *99*, 84.
(32) (a) Slater, J. C. *Quantum Theory of Molecules and Solids*; McGraw-Hill: New York, 1974; Vol. 4, Self-Consistent Field for Molecules and Solids. (b) Vosko, S. H.; Wilk, L.; Nusair, M. *Can. J. Phys* **1980**, *58*, 1200.
(33) Stoll, H.; Golka, E.; Preuss, H. *Theor. Chim. Acta* **1980**, *55*, 29.

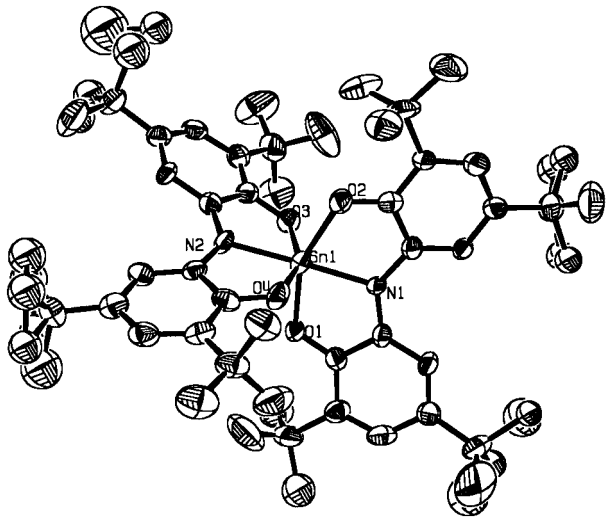

Figure 1. ORTEP drawing of the $Sn(CatNSQ)_2$ complex.

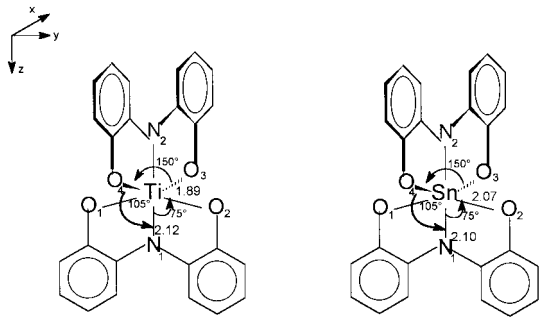

Figure 2. Model complexes and relevant geometrical parameters.

have been reported previously.[18] The complexes have been found to be paramagnetic with a $S = 1$ state as the ground state. A singlet state was found to lie 56(1) and 23(1) cm^{-1} above the ground state in the titanium and tin derivatives, respectively. The electronic spectra are characterized by a series of bands below 22 000 cm^{-1} and a series of band around 27 000 cm^{-1} assigned to ligand-to-ligand charge transfer transitions. In the complex $Ti(CatNSQ)_2$ an additional band around 24 000 cm^{-1} was assigned to ligand-to-metal charge transfer transitions.

Electronic Structure. All of the calculations were performed on model complexes in which the phenyl rings of $CatNSQ^{2-}$ were taken as coplanar and substituting the *tert*-butyl groups with hydrogen atoms. The model complexes and their relevant geometrical parameters are shown in Figure 2. The bond distances and angles were fixed to average values seen in the crystal structures. The overall nuclear symmetry of the model complexes is, therefore, C_{2v}, and all of the calculations were performed in this symmetry.

Searching for magnetostructural correlations, we have not attempted to locate the equilibrium geometries, but the effect of the main geometrical parameters' variations (namely, the M−O and M−N bond distances) on the electronic structure of the complexes was investigated.

The computed energy levels of the $S = 1$ state near the Fermi level for $Ti(CatNSQ)_2$ and $Sn(CatNSQ)_2$ are shown in Figures 3 and 4, respectively. The contributions of the metal and donor atoms expressed as gross atomic orbital populations to selected one-electron levels are shown in Tables 3 and 4 for $Ti(CatNSQ)_2$ and $Sn(CatNSQ)_2$, respectively. In both cases the SOMOs are degenerate b_1 and b_2 orbitals which, in D_{2d} symmetry, are the components of a doubly degenerate e species. The contour plots of the $19b_1$ and $19b_2$ orbitals for $Ti(CatNSQ)_2$ are shown in Figure 5. These orbitals are mainly localized on the two orthogonal $CatNSQ^{2-}$ radicals with main contributions of the 2p atomic orbitals of the N and O atoms. A small, but significant, amount of electron density is transferred onto 3d orbitals of titanium and onto 2p orbitals of the oxygen atoms of the orthogonal $CatNSQ^{2-}$ ligand. The oxygen contribution to the $19b_2$ orbital is a linear combination of $2p_y$ and $2p_z$ orbitals of the $CatNSQ^{2-}$ ligand which lies in the *yz* plane. The oxygen contribution to the $19b_1$ orbital is a linear combination of $2p_x$ and $2p_z$ orbitals of the $CatNSQ^{2-}$ ligand which lies in the *xz* plane. The lowest unoccupied orbitals shown in Figure 3 are mainly 3d titanium orbitals. A similar situation is found for the SOMOs of $Sn(CatNSQ)_2$, $20b_1$ and $20b_2$. The contour plots of these orbitals are shown in Figure 6. The molecule is viewed in the *xy* plane in order to evidence the contribution of the $4p_x$ and $4p_y$ orbitals of Sn. In this complex, in fact, electron density is transferred into empty 4p orbitals of tin, the 4d ones being too high in energy to significantly contribute to the composition of the SOMOs. The SOMO−LUMO energy gap is significantly greater than that computed for the titanium complex.

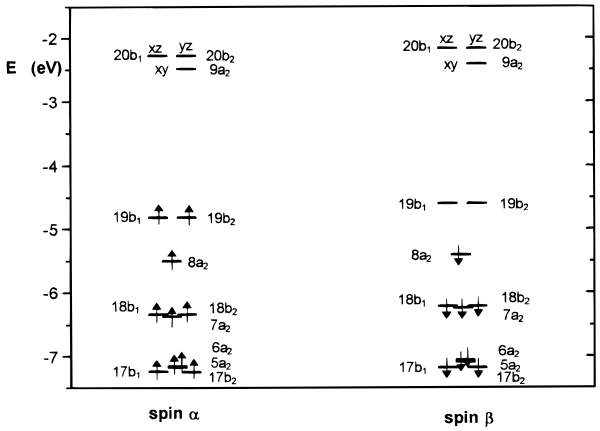

Figure 3. Computed energy levels of the triplet state near the Fermi level for the $Ti(CatNSQ)_2$ complex.

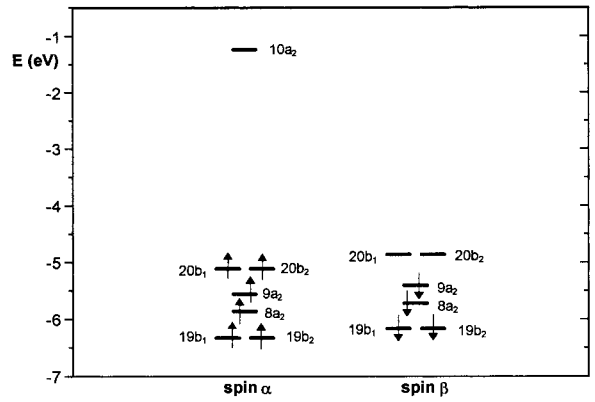

Figure 4. Computed energy levels of the triplet state near the Fermi level for the $Sn(CatNSQ)_2$ complex.

Electronic transitions have been computed for $Ti(CatNSQ)_2$ and $Sn(CatNSQ)_2$ using a ΔSCF procedure such as one-electron excitation from the orbitals shown in Figure 3. The results of the calculations are collected in Tables 5 and 6 and compared to the experimental data. The transitions calculated in this way correspond to spin-allowed triplet−triplet transitions. Only the transitions which are symmetry allowed in C_{2v} have been calculated. For the transitions involving degenerate orbitals, which would span an e representation in the highest D_{2d} symmetry group of the complexes, only one component has been computed. The overall agreement with the experimental data

Table 3. Percentual Gross Atomic Orbital Population for the Frontier Orbitals of $Ti(CatNSQ)_2$

	Ti		Ligand 1			Ligand 2						
A_2												
	d_{xy}		p_xO_1		p_xO_2	p_yO_3			p_xO_4			
$7a_2$	11.3		3.16		3.16	3.16			3.16			
$8a_2$	0.00		9.90		9.90	9.90			9.90			
$9a_2$	63.6		1.88		1.88	1.88			1.88			
B_1												
	d_{xz}	p_x	p_xN_1	p_xO_1	p_xO_2	p_xN_2	sO_3	sO_4	p_xO_3	p_xO_4	p_zO_3	p_zO_4
$18b_1$	.03	.23	6.28	8.68	8.68	.00	.01	.01	.08	.08	.00	.00
$19b_1$	4.70	1.45	16.53	6.00	6.00	.00	.00	.00	.95	.95	.29	.29
$20b_1$	74.0	.15	1.13	1.42	1.42	.03	.00	.00	6.82	6.82	.33	.33
B_2												
	d_{yz}	p_y	p_xN_1	sO_1	sO_2	p_yO_1	p_yO_2	p_zO_1	p_zO_2	p_yN_2	p_yO_3	p_yO_4
$18b_2$	.03	.23	.00	.01	.01	.08	.08	.00	.00	6.28	8.68	8.68
$19b_2$	4.70	1.45	.00	.00	.00	.95	.95	.29	.29	16.53	6.00	6.00
$20b_2$	74.0	.15	.03	.00	.00	6.82	6.82	.33	.33	1.13	1.42	1.42

Table 4. Percentual Gross Atomic Orbital Population for the Frontier Orbitals of $Sn(CatNSQ)_2$

	Sn		Ligand 1			Ligand 2						
A_2												
	d_{xy}		p_xO_1		p_xO_2	p_yO_3			p_xO_4			
$8a_2$	0.05		7.89		7.89	7.89			7.89			
$9a_2$	0.00		10.05		10.05	10.05			10.05			
$10a_2$	0.00		0.305		0.305	0.305			0.305			
B_1												
	p_x		p_xN_1	p_xO_1	p_xO_2	p_xN_2	sO_3	sO_4	p_xO_3	p_xO_4	p_zO_3	p_zO_4
$19b_1$	0.03		12.99	7.69	7.69	.00	.00	.00	.20	.20	.02	.02
$20b_1$	3.24		20.29	8.69	8.69	.00	.01	.01	.70	.70	.00	.00
B_2												
	p_y		p_xN_1	sO_1	sO_2	p_yO_1	p_yO_2	p_zO_1	p_zO_2	p_yN_2	p_yO_3	p_yO_4
$19b_2$	0.03		.00	.00	.00	.20	20	.02	.02	12.99	7.69	7.69
$20b_2$	3.24		.00	.01	.01	.70	.70	.00	.00	20.29	8.69	8.69

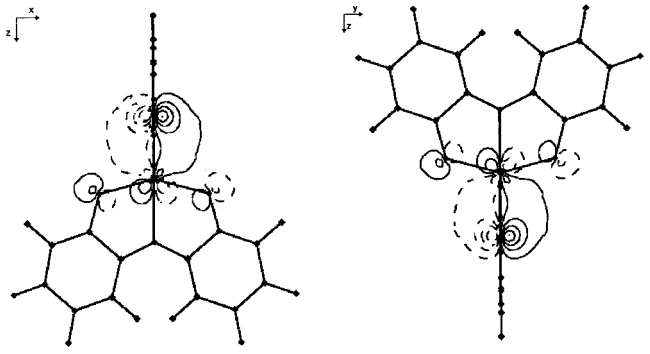

Figure 5. Contour plot of the SOMO orbitals, $19b_1$ (left) and $19b_2$ (right), of $Ti(CatNSQ)_2$.

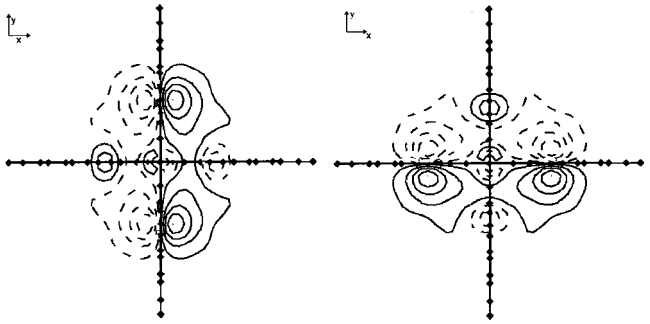

Figure 6. Contour plot of the SOMO orbitals, $20b_1$ (left) and $20b_2$ (right), of $Sn(CatNSQ)_2$.

is good for the titanium complex. For this derivative, the low-energy transition observed at 9800 cm^{-1} (computed at 8078 cm^{-1}) is assigned as $^3A_2 \rightarrow {}^3B_2$ and corresponds to a ligand-to-ligand charge transfer in agreement with the conclusions of Dei et al.[18] The transition observed at 23 900 cm^{-1} (computed at 26 868 cm^{-1}) is assigned to the $^3A_2 \rightarrow {}^3A_2$ and is essentially a ligand-to-metal charge transfer, again in agreement with the experimental observation.[18] The energies of the electronic transitions calculated for the tin derivative are all ligand-to-ligand transitions, in agreement with the experimental assign-

Table 5. Electronic Transition Energies (cm^{-1}) for $Ti(CatNSQ)_2$

transition	states	computed	exptl
$8a_2 \rightarrow 19b_2$	$^3A_2 \rightarrow {}^3B_2$	8 078	9 800
$18b_2 \rightarrow 19b_2$	$^3A_2 \rightarrow {}^3A_2$	13 645	14 200
$7a_2 \rightarrow 19b_1$	$^3A_2 \rightarrow {}^3B_1$	16 990	17 300/18 600
$8a_2 \rightarrow 9a_2$	$^3A_2 \rightarrow {}^3A_2$	26 868	23 900
$8a_2 \rightarrow 20b_1$	$3A_2 \rightarrow {}^3B_1$	31 096	28 200/30 400
$18b_1 \rightarrow 20b_1$	$^3A_2 \rightarrow {}^3A_2$	39 772	35 900

Table 6. Electronic Transition Energies (cm^{-1}) for $Sn(CatNSQ)_2$

transition	states	computed	exptl
$9a_2 \rightarrow 20b_1$	$^3A_2 \rightarrow {}^3B_1$	5 768	9 900
$19b_2 \rightarrow 20b_1$	$^3A_2 \rightarrow {}^3A_2$	11 038	14 800
$8a_2 \rightarrow 20b_1$	$^3A_2 \rightarrow {}^3B_1$	17 018	17 900/19 200
$20b_1 \rightarrow 10a_2$	$^3A_2 \rightarrow {}^3B_1$	31 968	26 000
$9a_2 \rightarrow 10a_2$	$^3A_2 \rightarrow {}^3A_2$	35 371	27 400/30 900 35 100

ment. The quantitative agreement with the observed data is not so good as that obtained for the titanium complex, but still satisfactory.

The calculation of the multiplets lying close to the ground state, which are responsible for the observed temperature dependence of the magnetic susceptibility of both $Ti(CatNSQ)_2$ and $Sn(CatNSQ)_2$, was performed using the single determinant (SD) formalism. This method is based on the decomposition of the energies arising from the occupation of a set of one-electron orbitals (*active orbitals*) into a sum of energies of single Slater determinants. This procedure has been described in detail in previous papers.[34,35] Since the magnetic orbitals (SOMOs) are rather well separated in energy from other one-electron levels, only these two orbitals were considered to be the active orbitals. The single determinants arising from the distribution of the two active electrons among these orbitals are shown in Chart 2. Four multiplet states arise: $^3A_2$, $^1A_2$, and two $^1A_1$. The energies of the A_2 states can be expressed as a sum of energies of single determinants according to

$$E(^3A_2) = E(|b^+c^+|)$$

$$E(^1A_2) = 2E(|b^+c^-|) - E(|b^+c^+|) \qquad (1)$$

considering that $E(|b^+c^-|) = E(|b^-c^+|)$. The energies of the $^1A_1$ states are obtained by the diagonalization of the 2×2 matrix

$$\begin{bmatrix} E(|b^+b^-|) & E(|b^+c^-|) - E(|b^+c^+|) \\ E(|b^+c^-|) - E(|b^+c^+|) & E(|c^+c^-|) \end{bmatrix} \qquad (2)$$

When applying eqs 1 and 2, we neglect the contributions of the excited charge transfer states to the energies of the multiplets. In the present case, eq 1 coincides with the approximate spin projection technique often used in the literature for computing the energies of the multiplets lowest in energy for weakly interacting systems.[25]

This approximation considers only the active magnetic electrons and can be considered as good as a CAS(2,2) calculation. This approximation was tested against rather complete CI calculations for describing the exchange interaction between a copper(II) complex and a nitroxide radical and was found to give results very close to those obtained by CI calculations.[25] Inclusion of excited configurations via a direct calculation of the two-electron integrals[34,35] should constitute the improvement of the method.

Chart 2

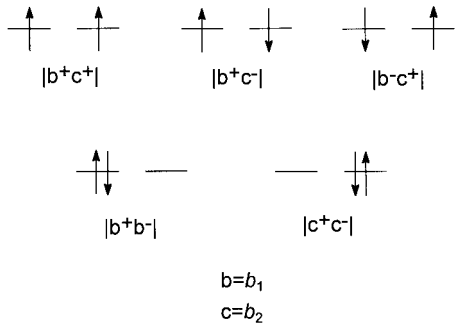

Table 7. Computed Multiplet Structure for $Ti(CatNSQ)_2$ and $Sn(CatNSQ)_2$

	ΔE^a_{calc} (cm^{-1})	
state	Ti	Sn
$^3A_2$	0	0
$^1A_2$	57 [56(1)]	58 [23(1)]
$^1A_1$	9510	11 934
$^1A_1$	9571	11 991

[a] The energies are computed as differences from the ground $^3A_2$ state. The experimental values are in square brackets.

The results of the calculations for $Ti(CatNSQ)_2$ and $Sn(CatNSQ)_2$ are shown in Table 7. In any case the $^3A_2$ state is the ground state and the next excited state is $^1A_2$. The other singlet states, which correspond to ligand-to-ligand charge transfers, are computed at higher energies. The singlet−triplet splitting for the titanium derivative is in quantitative agreement with the experimental value while a larger value is computed for the tin complex. As already stated, since we use some idealization of the real molecular symmetry, we do not expect from these calculations a full quantitative agreement with the experimental findings, and the result for the tin complexes can be fortuitous, only the order of magnitude of the exchange coupling constant being meaningful. In fact, the singlet−triplet splitting or, in general, magnetic properties are influenced by the real structure of the systems and also by more subtle effects such as the solid state packing. The well-known $[Cu_2Cl_6]^{2-}$ systems[25] are indicative of these facts: the values of the exchange coupling constant, J, were found to be influenced by the nature of the counterions which modulate very subtle structural changes and were quantitatively reproduced only by dedicated ab initio CI calculations[27] at the expense of a lot of computer resources. With the aim of looking at the influence of structural deformations on the singlet−triplet energy gap, while preserving the overall C_{2v} symmetry of the molecule, we have performed calculations by varying the M−O and M−N bond distances. The differences between the energies of $^3A_2$ and $^1A_2$ computed with eq 1 for different values of M−O and M−N distances, embracing the extreme values seen in the crystal structures of the reported complexes, are graphically shown in Figure 7. The computed energy difference is strongly dependent on the M−O distance but not significantly affected by the variation of the M−N distance. The triplet state is stabilized at longer M−O distances. At the same value of the M−O distance, the singlet−triplet gap computed for $Sn(CatNSQ)_2$ is always smaller than that computed for $Ti(CatNSQ)_2$. The singlet−triplet gap computed for $Sn(CatNSQ)_2$ is also less sensitive to the variation of the M−O distance than that of $Ti(CatNSQ)_2$. The largest effect observed on the

(34) Daul, C. A. *Int. J. Quantum Chem.* **1994**, *52*, 867.
(35) Daul, C. A.; Doclo, K.; Stückl, C. A. In *Recent Advances in Density Functional Methods*; Chong, D., Ed.; World Scientific Publishing Company: Singapore; Part II, in press.

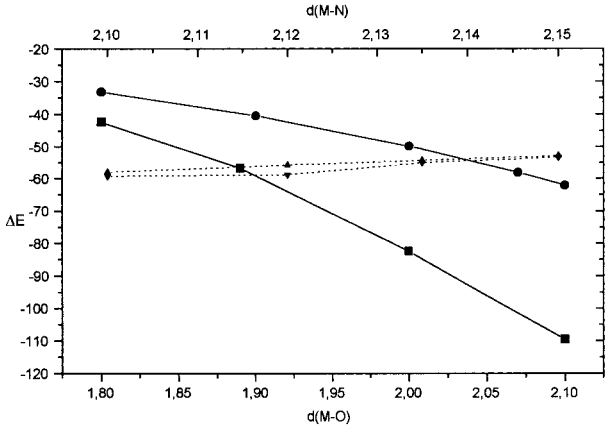

Figure 7. Dependence of the $\Delta E(^3A_2-{}^1A_2)$ on the distances Ti−O (■) and Sn−O (●) in Å for d(Ti−N) = 2.12 Å and d(Sn−N) = 2.10 Å, bottom, and on the distances Ti−N (▲) and Sn−N (▼) in Å for d(Ti−O) = 1.89 Å and d(Sn−O) = 2.07 Å, top.

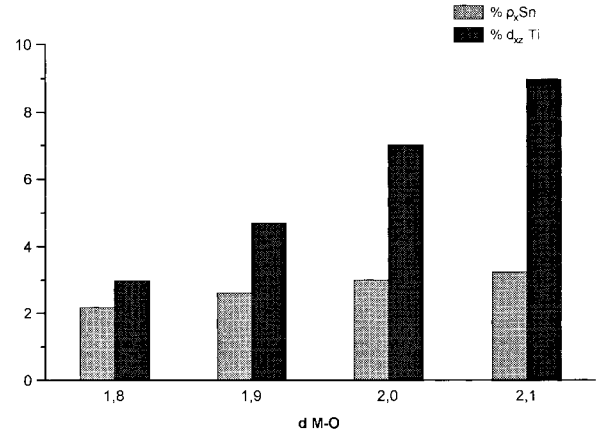

Figure 8. Dependence of the percent contribution of the metal orbitals to the $20b_1$ and $19b_1$ orbitals of Sn(CatNSQ)$_2$ and Ti(CatNSQ)$_2$ on the metal−oxygen distance in Å.

composition of the magnetic orbitals by varying the M−O bond distance is the variation of the metal orbital contribution. This is shown in Figure 8 for the b_1 SOMOs of the two complexes. The same trend is computed for the b_2 SOMOs. Upon increasing the M−O bond distances the antibonding character of the M−O interactions decreases and the magnetic orbitals become more metal centered. The singlet−triplet gap is computed to be more dependent on the M−O distance in the titanium complex than in the tin derivative. This observation can be rationalized by considering that the metal contributions to the SOMOs are greater for titanium than for tin.

The composition of the magnetic orbitals (Figures 5 and 6) evidences two main contributions to the exchange pathway responsible for the stabilization of the $^3A_2$ state, namely, a direct contribution and a superexchange contribution. The direct contribution comes from the computed delocalization of the electronic density, mainly localized on one of the two $CatNSQ^{2-}$ moieties, onto oxygen orbitals belonging to the other orthogonal ring. This contribution is ferromagnetic as long as the two ligands lie in orthogonal planes. The superexchange contribution comes from the computed delocalization of the electronic density onto the metal orbitals d_{xz} and d_{yz} for the titanium derivative and p_x and p_y for the tin one. As long as the orbitals remain orthogonal (C_{2v} or C_2 symmetries), also this contribution to the exchange interaction is ferromagnetic. Both of these effects, therefore, stabilize the $^3A_2$ state compared to the singlets. The computed dependence of the singlet−triplet splitting on the metal−oxygen distance can be attributed to the variation of the metallic composition of the SOMOs (the other atomic orbital composition remaining almost constant) and allows us to conclude that the superexchange mechanism is more important than the direct one to determine a ferromagnetic interaction. This ferromagnetic exchange pathway is more efficient when 3d orbitals are involved. For this reason, the $^3A_2$ state is always more stabilized in the titanium derivative than in the tin one, independent of the actual geometrical parameters.

Conclusions

The spectromagnetic properties of Ti(CatNSQ)$_2$ and Sn(CatNSQ)$_2$ have been reproduced by DF calculations with a satisfactory agreement with the experimental data. In particular, the nature of the exchange pathways which stabilizes the ferromagnetic state has been ascertained as mainly due to the delocalization of unpaired spin density from the radicals into two orthogonal metal-centered orbitals. The SD method for computing the singlet−triplet splitting is found to reproduce the order of magnitude of the experimental magnetic coupling constant and is becoming a fast and efficient method of calculation of multiplet energies which fully exploits the symmetry of the system. The computed singlet−triplet splitting matches perfectly the observed experimental value for Ti(CatNSQ)$_2$, while that of Sn(CatNSQ)$_2$ is largely overestimated. A better agreement for the Ti electronic transition energies, compared to those for the tin derivative, is also found. Probably, this is due to the larger distortion from the coplanarity of the benzene rings observed for the tin complex. Moving the aromatic rings of the ligands away from coplanarity (and consequently reducing the overall molecular symmetry to C_1) removes the strict orthogonality of the magnetic orbitals, allowing for antiferromagnetic contributions to the exchange interactions.

The SD method of calculation will be applied to the characterization of other metal−radical systems. In particular, attention will be paid to the description of the exchange interactions in tris(semiquinonato) metal(III) complexes, in which both ferro- and antiferromagnetic interactions seem to operate according to the nature of the metal,[36,37] in order to describe in terms of orbital interactions the exchange pathway as already done for the M(CatNSQ)$_2$ (M = Sn, Ti) complexes.

Acknowledgment. Thanks are expressed to Dr. A. Caneschi, Università di Firenze, for collecting the X-ray diffraction data, to Prof. A. Dei for helpful and stimulating discussions, and to Prof. D. Gatteschi for his encouragement during the work.

Supporting Information Available: Tables containing data collection information, positional and thermal parameters for all atoms, interatomic distances and angles, and anisotropic thermal parameters for Sn(CatNSQ)$_2$ (9 pages). Ordering information is given on any current masthead page.

IC970906E

(36) Adams, D. M.; Rheingold, A. L.; Dei, A.; Hendricksin, D. N. *Angew. Chem., Int. Ed. Engl.* **1993**, *32*, 391.
(37) Lange, C. W.; Conklin, B. L.; Pierpont, C. G. *Inorg. Chem.* **1994**, *33*, 1276.